Spark Plasma Sintering of Binderless *n*-WC and *n*-WC- X (X=Nb, Re, Ta, Ti, B, Si)†

KUMAR A K Nanda*, WATABE Masaaki, YAMAUCHI Akira*, KOBAYASHI Akira ***, and KUROKAWA Kazuya***

Abstract

Nano sized tungsten carbide (n-WC) compacts with and without grain growth inhibitors were synthesized by Spark Plasma Sintering (SPS) with different heating rates. The microstructure and mechanical properties of the various samples were compared. Grain growth inhibition effects increased in the order Nb>Re>Ta>Ti and with increasing heating rate. Addition of Si and B increases grain growth, but suppresses the formation of the brittle semi carbide (W_2C) phase. Using the WC-X phase diagram and the sintering rate curves, we try to generalize the effect of various grain growth inhibitors on the sintering of n-WC.

KEY WORDS: (Spark Plasma Sintering), (Nano tungsten carbide), (Microstructure), (Mechanical properties), (Grain growth inhibition), (Heating rates)

1. Introduction

Carbides of the refractory transition metals have been commonly employed for applications requiring high hardness, stiffness, wear resistance and abrasion resistance. WC cermets containing the hard carbide phase and Co or Ni binders anywhere between 4-30 wt% have been routinely synthesized by a number of metallurgical production methods[1-4]. Their requirements arise primarily in the machining and drilling industries and also in the preparation of dies for optical lenses. However, in recent years, attention has shifted to the synthesis of nano-grained WC compacts which result in increased hardness induced by the Hall-Petch effect. Presence of a binder in such nano grained structures increases the tendency for grain growth of the hard carbide phase by wetting, surface diffusion and viscous flow at the interfacial area between carbide particles. Yet, it offers significant advantage in terms of increased fracture toughness from 5 MPa-$m^{1/2}$ (no binder) to 14 MPa-$m^{1/2}$ (for WC-14 wt% Co) [5, 6]. Hence a persistent challenge in this field has been the proper choice of the binder and the fraction of the binder phase in the final microstructure so that a dense, nano grained microstructure with high hardness and fracture toughness can be obtained.

In addition to these challenges, even without the binder phase the WC system poses certain inherent problems during consolidation from the powder material: abnormal grain growth[7], faceting and anisotropic growth[8], growth of the carbon – deficient phases (W_2C and WC_{1-x}) [9] and poor oxidation resistance[10]. Increased carbon content – for instance at the graphite die / sample interface – abets abnormal grain growth during sintering. Faceting and anisotropic growth occur by grain rotation, re-precipitation and coarsening along the low energy planes of the individual crystallites due to the difference in surface energies between the (10-10) and (0001) planes. Surface oxidation and ternary element reactions aid the loss of carbon leading to the non stoichiometric WC phases in the microstructure. The oxidation resistance of WC assumes importance in industrial applications where the initial microstructure and properties have to be retained at elevated temperatures exceeding 500 C. The occurrence of the above phenomena results in a degradation of the final mechanical properties.

Hence, achieving a constrained grain size, homogenous microstructure and improved mechanical properties together with minimized binder composition are the fundamental aims of current research on WC based cemented carbides. In this paper, we report certain experiments on the compaction of binderless WC and WC – 1wt% X (where X = Ta, Ti, Si, Nb, Cr, Re or B) by Spark Plasma Sintering (SPS). The microstructural parameters and mechanical properties have been evaluated and compared. We also discuss the sintering behavior of the various samples to provide explanations for the observed microstructure.

† Received on June 11, 2010
* Hokkaido University
** Ohta Seiki Co. Ltd.
*** Associate Professor

Transactions of JWRI is published by Joining and Welding Research Institute, Osaka University, Ibaraki, Osaka 567-0047, Japan

2. Experimental Details

Nano sized WC powders were purchased from M/s. Allied Materials, Japan. The particle size measured by BET was 70 nm and the powder composition included 0.4% O, 5 ppm Cr, 27 ppm Fe, 4 ppm Mo, 3 ppm Ca, 2 ppm Ni, <5 ppm Si and < 2 ppm Sn. The WC powder was mixed with 1 wt% Si, B, Nb, Ta, Re or Ti in a planetary ball milling unit for 30 minutes. X-ray diffraction of the powders did not reveal the formation of any new phases after milling. Approximately 2.5 – 3 g of these powders was filled into a 10 mm diameter graphite die for SPS. Graphite spacers were used to separate the powder sample from the punch and die. Sintering was carried out in vacuum (< 4 Pa) with three different heating routines: (i) 50 C/min at 50 MPa from 600 C to 1800 C, (ii) 150 C/min at 50 MPa from 600 C to 1800 C and (iii) 150 C/min at 50 MPa from 600 C to 1350 C and 50 C/min at 60 MPa from 1350 C until 1600 C, the pressure being increased from 50 to 60 MPa within 15-20 seconds. For each of the above routines, the initial part of the heating program was similar: from RT to 600 C at 4 C/min and soaking at 600 C for 3 minutes. Also, in all the routines the peak temperature was held constant for 10 minutes before being cooled down. These routines are shown in **Fig. 1** and samples prepared with each of these techniques were labeled as either WCX1, 2 or 3.

Sintering was stopped when the measured shrinkage showed no change in values for 2 consecutive readings, after which the pressure on the punch was released and the sample was cooled to room temperature in vacuum. Samples were polished with monocrystalline diamond paste to a mirror finish after which their densities were measured by the Archimedes method. Later, they were characterized by X-ray diffraction and Vickers hardness testing. Finally, the samples were fractured and their fractured surfaces were observed by Field Emission SEM.

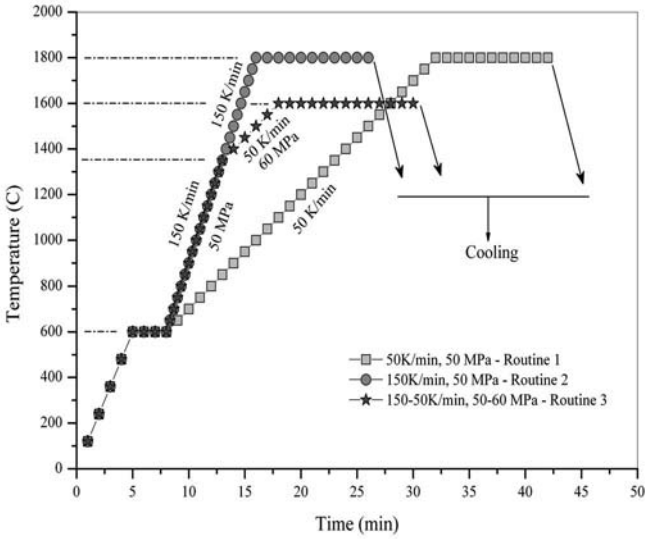

Fig. 1 Time-Temperature profile of the heating routines.

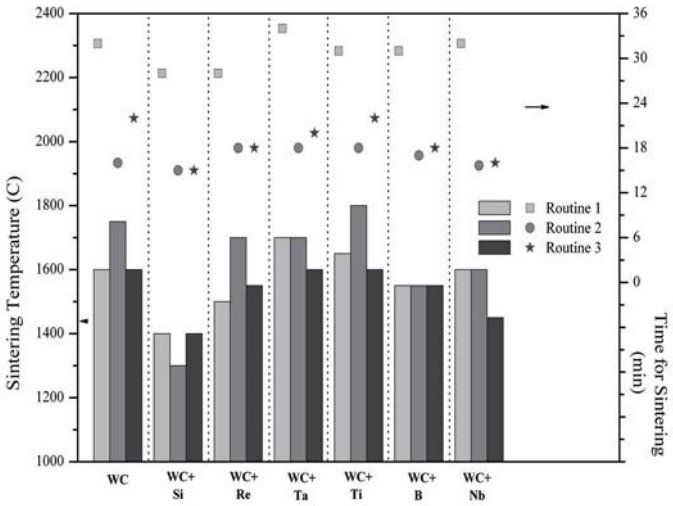

Fig. 2 Sintering temperature and total sintering time of the various samples.

3. Results

3.1 Sintering behavior

During the heating stage up to 600 C, all the samples showed an initial expansion (decrease in shrinkage) which can be attributed to the release of trapped gaseous atoms and also to thermal expansion of the powders[8]. Densification (increase in shrinkage) began at around 850 – 950 C in all the samples. However, the temperature at which sintering was completed varied with the samples and the heating rates. The sintering temperatures were also found to be sensitive to the background pressure. **Figure 2** compares the sintering temperatures and time for densification of the samples. Heating routine 3, in which the pressure was increased from 50 MPa to 60 MPa, seemed to decrease the sintering time and temperature for most of the samples. However, WC-B showed no difference in sintering temperature in any of these heating programs while WC-Si showed only a minor difference.

3.2 Density

The densities of the sintered WC powder as evaluated by the Archimedes method are shown in **Fig. 3**. Except for WC-Ti, WC-Si and WC-B the other samples showed a relative density of more than 95% of the theoretical value as shown in the top part of Fig. 3.

Pure WC, WC-Ta and WC-Re showed 100% densification, implying that SPS can be used with proper combinations of heating rates and pressure for achieving complete densification. However, WC-Si showed 95% densification while WC-B showed only 85% densification irrespective of the heating routine adopted. WC-Ti showed lower density with increasing sintering temperature.

3.3 X-ray diffraction analysis

The X-ray diffractograms of the samples did not show any difference with the heating routines. However,

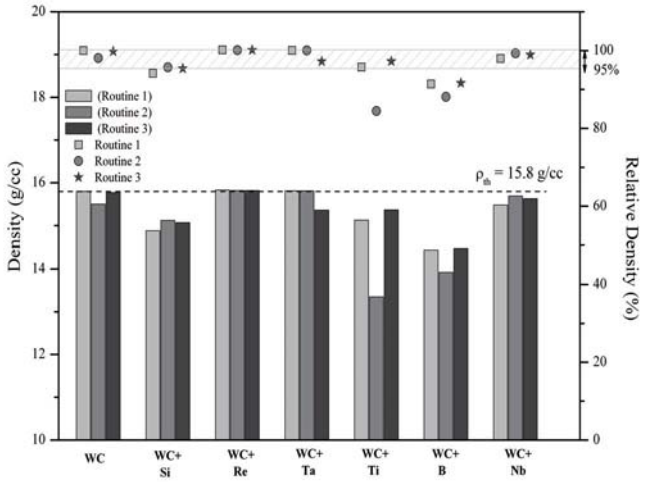

Fig. 3 Density and Relative density of the various sintered samples.

between the samples there were interesting differences in their structural transformations. **Figure 4** shows the XRD of the samples carried out with heating routine 3. Sintered WC samples showed the presence of the semicarbide phase, W_2C. Similar semicarbide formation was also found for WC-Re, WC-Nb and WC-Ta. In a recent report by Zhang et al[9] the synthesis of dense WC compacts by SPS with similar heating rates had resulted in a microstructure dominated by W_2C and WC_{1-x} phases unless the C content in the powders was increased.

Using the present method we find that the WC_{1-x} does not form and the relative diffraction intensity ratio between the strongest WC and W_2C reflections is less than 10:1. However, in WC-Ti, WC-B and WC-Si the semicarbide phase was completely suppressed but new phases were detected. In WC-Ti, the W-rich WC_{1-x} was detected. In WC-B, WB phase was observed while W_5Si_3 and WSi_2 were detected in the WC-Si sintered samples. The suppression of W_2C is almost always accompanied by the formation of another phase.

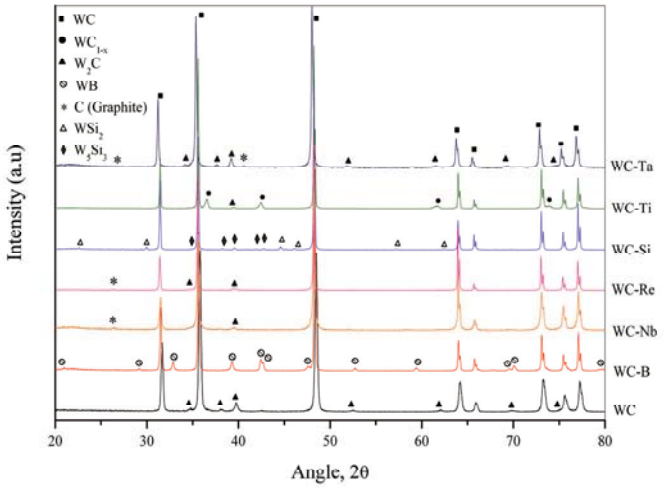

Fig. 4 XRD of the samples sintered with heating routine 3.

3.4 Microstructure

Fractured specimens were used for the microstructure studies. FE-SEM images of the fractured cross sections were used to determine the grain size using an image processing tool (Image Pro 6.1). Approximately 30-70 grains from each location of a sample was randomly selected for the measurements. The boundaries were delineated manually and the average diameter (average length of the diameters measured at 2° intervals and passing through the centroid of the selected grain) of the grains were calculated. The grain size of the samples was normally distributed but was also positively skewed for most samples. A representative histogram of the WC-Si sample (with skewness value of + 4.8) is shown in **Fig. 5**. Almost 90% of the total number of grains analysed lie within 250 nm – 1 μm while a few grains exceed an average diameter of 1.5 μm. As mentioned earlier, inhomogeneous grain size distribution (owing to either anisotropic or abnormal grain growth) leads to ambiguity in the grain size measurement of nano crystalline WC. Measures of variation from the average values are hence important to correlate the properties with the microstructure of the samples. **Figure 6** shows the grain sizes of the various samples with the bars representing

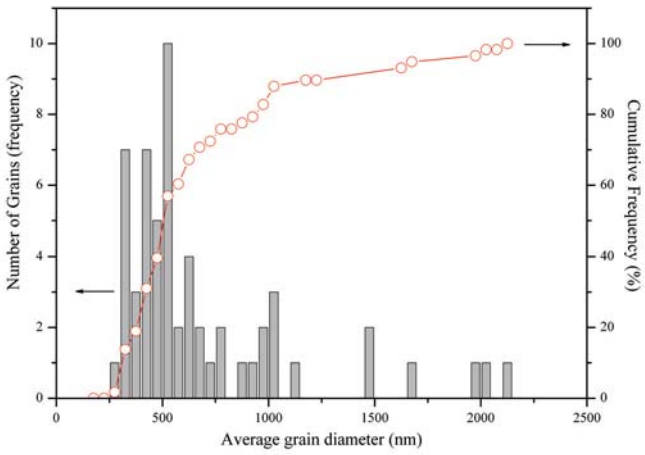

Fig. 5 Grain size distribution in sintered WC-Si3 sample.

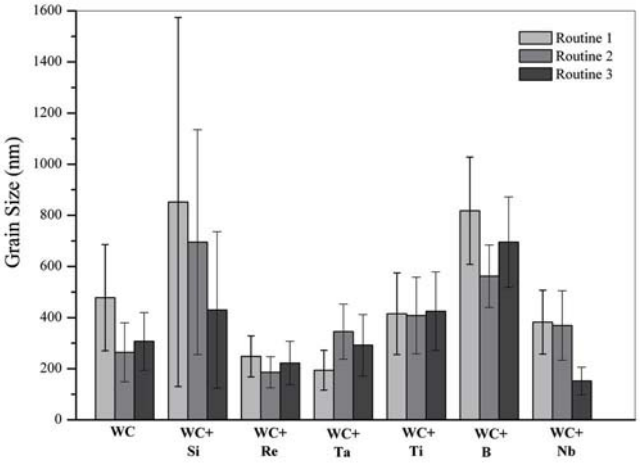

Fig. 6 Grain sizes of the various sintered samples.

the standard deviation, sd (in nm). Particularly in the case of WC-Si, the sd was very high owing to the non uniformity of the grain size and the anisotropic structure.

Cross sectional FESEM images of the fractured samples are shown in **Fig. 7** and discussed below:

For the pure WC samples, heating routine 1 leads to abnormal grain growth. The microstructure was populated by longitudinal grains measuring around 2 μm along their lengths and 300-400 nm in the transverse direction. In addition, smaller grains measuring around 300 nm in diameter were also observed. However, pure WC under heating routine 2 seemed to exhibit a lesser amount of abnormal growth behavior. The average grain size was also reduced to < 250 nm. With heating routine 3, anisotropic growth was reduced and the average grain size was also restricted to 300 nm.

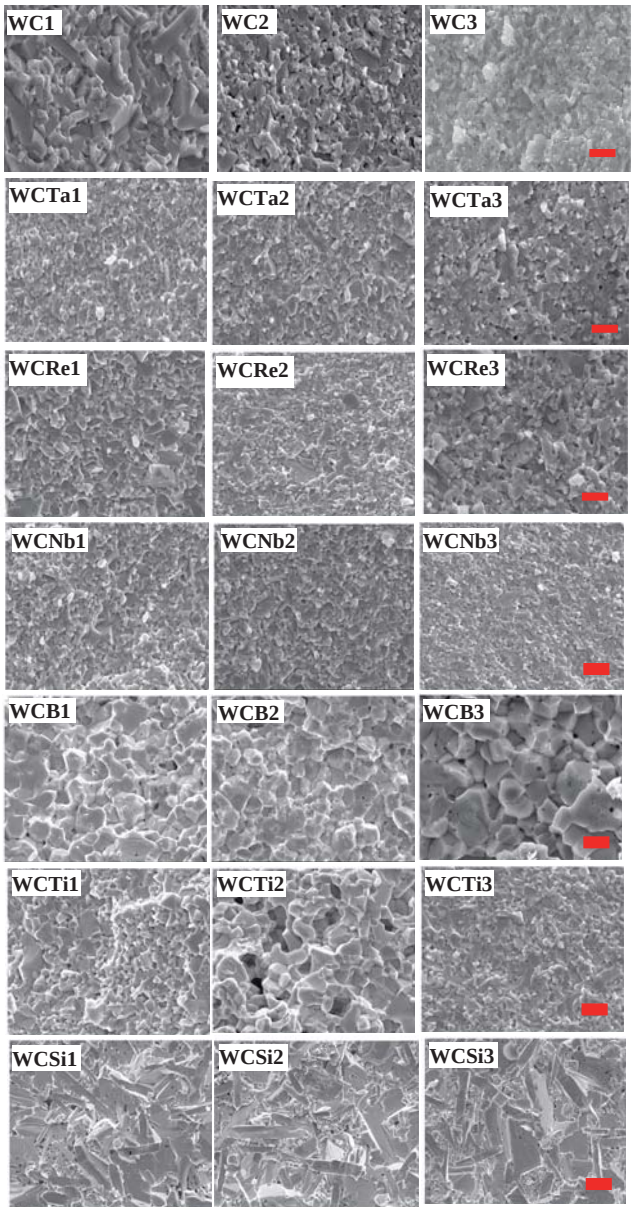

Fig. 7 Fractured surfaces of the samples (Distance markers in red represent 1 μm).

WC with Nb and Re additions showed almost similar microstructure to that of pure WC but a lesser fraction of abnormal grains. In WC-Nb, the effect of pressure was seen to be advantageous as the grain size was controlled to 160 nm with heating routine 3 compared to the other two routines which showed average grain size < 370 nm .

With WC-Re, the grain sizes were found to be fairly unaffected by the heating procedures as all the samples recorded nearly equal grain sizes of ~ 200 nm. WC-Ta also showed similar behavior. Generally, Nb, Re and Ta were found to be potentially good grain growth inhibitors.

WC with boron addition showed the largest grain growth (800 nm) among all the other samples with slow heating rate. Moreover, there was no abnormal growth observed in the microstructure. On increasing the heating rate from 50 to 150 C/min, the grain size was substantially reduced from 800 nm to 570 nm. With heating routine 3 the grain size again increased to 700 nm. Clear isolated pores along grain boundaries and grain surfaces were visible in the microstructure. Additionally, large inter-particle pores were also observed which can alter the density significantly.

The microstructure of WC-Ti consisted of an almost equal mixture of both small (~250 nm) and large (~450 nm) grains. The average grain size did not vary greatly between the heating routines and measured a constant value of ~ 400 nm. The microstructure of the WCTi2 samples showed large open porosity, similar to WC-B. This may be due to the fact that the high sintering temperature of the WCTi2 sample (~ 1750 C) could have caused the melting and evaporation of Ti or TiO_2 leaving voids in the matrix.

With the addition of Si, the anisotropic growth behavior of WC was greatly enhanced as shown in Fig. 7. The microstructure showed many thin plate-like crystals amidst smaller grains of ~ 200 nm size. The observed anisotropy was greater than that of pure WC. The shorter dimension was around 200-300 nm while the longer dimension was 1.5-2 μm and in some grains exceeded 4-5 μm. The aspect ratio varied between 3.5 and 4.8 for the different samples. Similar to WC-B, the microstructure was porous implying that densification was not complete but rather in the final stages of sintering.

3.5 Hardness and fracture toughness

The proposed ideal hardness of nano grained WC is 2955 HV with grain size < 100 nm[12]. However, the reported values of hardness of WC vary between 1200 HV[13] to over 2600 HV for pure binderless WC[14]. For the present experiments, the Vickers hardness of the samples was measured with a micro hardness tester (Mitutoyo Instruments) and the results are shown in **Fig. 8**. Depicted values are the average of 10 indentations under a load of 2 kgf.

Binderless WC, WC-Re, WC-Ta and WC-Nb showed high hardness of ~ 2700 HV2 while WC-Si, WC-B measured consistently lower hardness values of ~ 2000 HV2. All the samples exhibit improvement of hardness

with smaller grain size and higher heating rate. Apart from their microstructural dependence, the hardness was also found to be strongly dependent on the densification

and sintering temperatures. Particularly in the case of WC-Ti, the low density WC-Ti2 showed a very low hardness despite the increase in heating rate, due to high porosity. Measurement of the crack length after indentation was used to calculate the fracture toughness of the samples using the relation:

$$K_{Ic} = 0.203\ (c/a)^{-3/2}\ a^{1/2}\ H \qquad (1)$$

where 'c' is the crack length measured from the centre of the indentation, 'a' is the indentation diagonal length and H is the hardness. Fracture toughness of the samples determined by the above method is shown in **Fig. 9**. The K_{Ic} values varied between 3.9 MPa-$m^{1/2}$ for WC-B to 6.9 MPa-$m^{1/2}$ for the binderless WC samples.

Grain inhibitors like Nb, Re and Ta recorded very high hardness, but not a corresponding improvement in fracture toughness. Although one single cause cannot be attributed to the observed fracture toughness behavior, the general trend of variation in most of the samples

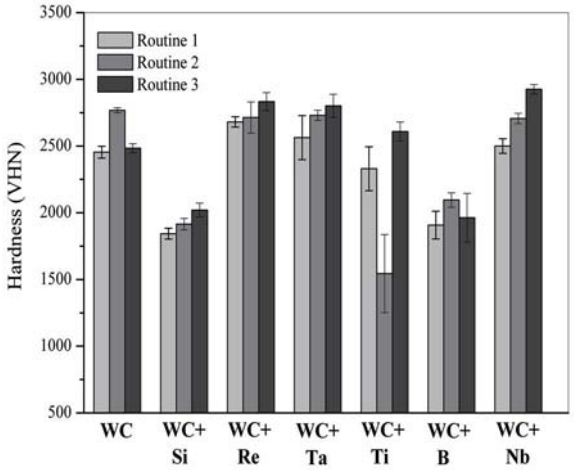

Fig. 8 Hardness of WC-1wt% X samples sintered under different conditions.

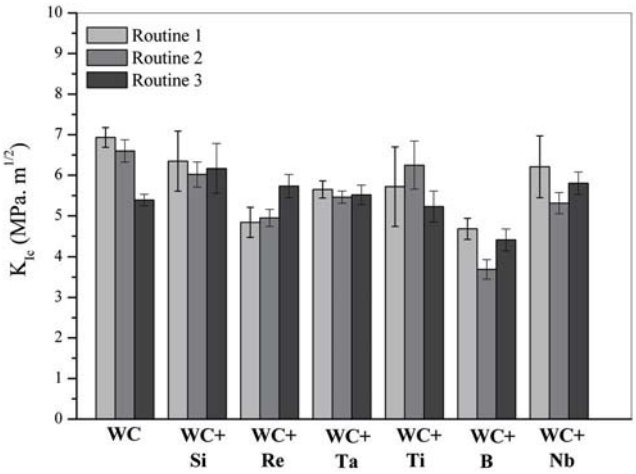

Fig. 9 Fracture toughness of the sintered samples.

suggest that under low heating rates the fracture toughness is improved.

This may be attributed to the large fraction of abnormal grains in those samples. Presence of abnormal grains has been reported to increase K_{Ic} of cemented WC by crack deflection, crack bridging and cutting of elongated grains[15]. Particularly in the case of binderless WC, slow heating rates (increased grain size) and a large fraction of abnormal grains in the microstructure increases the K_{Ic} values to 6.9 MPa-$m^{1/2}$ as compared to 5.3 MPa-$m^{1/2}$ in the other WC samples. The combined influence of high heating rate and pressure is also known to introduce high residual stress levels in the samples leading to low fracture toughness [16].

Another factor to be considered is that the semi carbide W_2C phase is brittle and when present, reduces the fracture toughness. In the case of WC-Si, the complete suppression of the W_2C phase may have led to a higher fracture toughness of the sample compared to those samples which contained the semi carbide phase. However, in WC-B which also did not contain the semi carbide phase, the generally large amount of porosity seemed to affect its fracture toughness adversely. WC-Re, Ta and Nb showed almost similar fracture toughening behavior with K_{Ic} ~ 5.5 MPa- $m^{1/2}$.

4. Discussion

Sintering is commonly characterized by two phenomena: densification and grain growth. In principle, there are 6 different mechanisms that may operate either sequentially or simultaneously (depending on the current sintering stage) leading to densification and grain growth[17]. In the sintering of nano WC, three sintering stages have been identified: i) rearrangement of particles without grain growth, ii) necking between the particles and iii) initial grain growth and pore elimination accompanied by massive grain growth[18]. However, this ideality is often upset by the presence of oxidation and reactions between the sintered species. Moreover, the contact Hertzian stresses are very large when the particle size is smaller than 100 nm adding to the driving force for sintering. The high contact stresses can cause localized yielding and plastic flow in very short time scales[11].

In the light of the present investigation, it is thus necessary to analyse the sintering mechanism and associate them with the observed microstructure and properties. Hence, the aim of this section is to discuss (a) the sintering behavior of nano-WC in response to the different processing schedules and (b) the development of microstructure and its effect on the properties of the samples. Since all the tests were carried out on the samples after completion of sintering, our analyses are based on the final chemical and microstructural equilibrium of the samples and no quantitative evaluation of the transformation kinetics is included.

4.1 Sintering behavior

In the high temperature sintering of WC, the

formation of the W-rich phase (W_2C) may be produced by two mechanisms: oxidation – reduction of WC and decomposition of the high temperature WC_{1-x} phase. In the former case, the mechanism proceeds as follows:

At high temperatures, owing to its high surface area, nano grained WC oxidises by any or a combination of the following reactions:

$2C + O_2 \longrightarrow 2CO$ (ΔG^o ~ -450 kJ/mol at 1000 C)
$C + O_2 \longrightarrow CO_2$ (ΔG^o ~ -390 kJ/mol at 1000 C)
$W + O_2 \longrightarrow WO_2$ (ΔG^o ~ -350 kJ/mol at 1000 C)

Among these, CO and CO_2 are lost to the atmosphere while tungsten oxide is retained in the sample. As sintering proceeds to higher temperatures, the oxides of tungsten also evaporate at ~ 1200 C due to their high vapour pressure. Some of the samples in which sintering was interrupted at low temperatures actually showed the presence of tungsten oxide [19]. However, the oxidation of W from WC cannot lead to the formation of W_2C. But, the decarburization of WC can lead to a W – rich microstructure which can stabilize by the formation of either the equilibrium W_2C phase (if the loss of carbon is high) or the WC_{1-x} phase (if the temperature is sufficiently high and the carbon loss is only moderate).

$$WC + W \longrightarrow W_2C$$

In the latter case, the eutectoid decomposition reaction of WC_{1-x} can also result in the formation of WC and W_2C phases. During the process of sintering, the WC phase being a stoichiometric line compound undergoes composition fluctuations either due to oxidation or by reaction with the binder phase leading to the formation of the high temperature α-WC_{1-x} phase which subsequently decomposes to WC and W_2C:

$$WC_{1-x} \rightleftharpoons WC + W_2C \quad (2530\ C)$$

However, in the presence of the binder phase, possibilities for oxidation of the binder also compete with the above discussed oxidative mechanisms. Additionally, the binder can also react with WC to form new carbides or compounds of tungsten. In the case of binder oxidation, examination of the Ellingham diagram suggests that oxides of B (B_2O_3), Si (SiO_2), Ti (TiO_2), Ta (Ta_2O_5) and Nb (Nb_2O_5) are more stable than oxides of W (WO_3, WO_2). However, their presence could not be detected in the sintered samples possibly due to evaporation and/or suppression by alternate reaction paths[18]. WC-B and WC-Si seem to show the latter mechanism whereby new phases WB and WSi_2 are formed rather than oxides of B or Si. Moreover, they provide an important route for suppressing the formation of the semi carbide phase W_2C through the oxidative mechanism discussed earlier by stabilizing the free W through alternate reactions.

Interestingly, the WC_{1-x} phase was detected only in the case of WC-Ti. This could be due to loss of carbon to form TiO_2 and TiC rather than oxidation of WC. TiC (ΔH_f ~ -180 kJ/mol) being more stable than WC (ΔH_f ~ -40 kJ/mol) also has very high solubility in WC as a substitutional solid solution (W,Ti)C (extended solubility to nearly 40 wt% WC in the solid phase at 1200 C)[20]. This lends stability to the WC-Ti system reducing the loss of carbon by the oxidative mechanism. The exothermic heat accompanying the formation of TiC also increases the temperature of the compact that results in the formation of the WC_{1-x} phase. However, elements like Nb that are capable of forming more stable carbides do not show such behavior possibly owing to their limited solubility in WC. In such cases, the oxidation-reduction reactions detailed earlier proceeds resulting in the formation of the semi carbide phase.

The final products after sintering of WC are thus seen to be chemically inhomogeneous with substantial amounts of secondary phases, W_2C (with WC-Nb, WC-Ta, and WC-Re samples), WC_{1-x} (as with WC-Ti) and WC-WSi_2 (with WC-Si) and WC-WB (with WC-B). These analyses provide us with information concerning the proper choice of ternary additions and their compositions to obtain pure WC composites with minimal secondary phases. Observation of the phase diagram of the W-C-X system (with X denoting the ternary additions) suggest that the phase diagrams involving W-C at the sintering temperatures of interest (~ 1500 C) can be classified into 2 general categories (**Fig. 10**).

We illustrate one general form of the equilibrium phase diagram of W-C-X in Fig. 10(a). The W-C composition line is magnified and the ternary end is truncated (dashed line) for clarity. The straight lines represent tie lines connecting the stable compounds/phases that can coexist. We start with an initial composition lying along the magnified a-WC region. During the process of sintering, the oxidation process alters the composition to a W-rich point - a'. This point lies in the field of the two phase region bounded by WC-W_2C and the a-b tie lines and hence the final compact is a mixture of both the phases. WC-Nb, Re, Ti and Ta follow such similar sintering routes yielding W_2C. The steeper is the tie line a-b, the more difficult it is to avoid the presence of W_2C (for instance in WC-Re). Also, the greater the initial oxidation of WC, the larger the fraction of the W_2C phase that forms. When the a-b tie line is not steep, and by a proper choice of initial composition, such that the initial point is at or above the composition a, the point a' can be made to fall into the phase field containing WC-XC. In such cases, the presence of the semi carbide phase can be minimized. In the commonly studied WC-Co system too, such deviations from the initial composition result in the formation of the η (carbide) phase or graphite inclusions[21]. It is worth mentioning that WC-Ti presents an interesting scenario since Ti has an extensive solubility in W. TiC-WC coexist over a comparatively substantial range of composition so that the small variations of WC (to a') can be accommodated within this region.

In the second case (Fig. 10(b)), the introduction of certain elements (B, Si) shift the equilibrium between

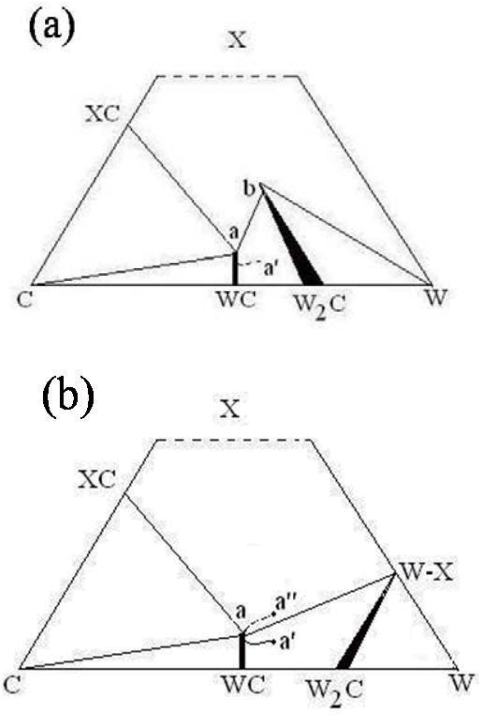

Fig. 10 General forms of the W-C-X phase diagram.

W_2C-WC to a more advantageous W_2C-WX line. This happens when W reacts readily with the ternary element thus shifting the equilibrium between the inter W-C phases. Any shift in the initial composition from WC will move the equilibrium into the triangular region bounded by WC-WX-W_2C (point a'). Such instances are observed when the fraction of the ternary addition is very small so as to lie well within the composition line denoted by WC-a (for instance in WC-1 wt% Al) [19]. The fraction of W_2C in the final microstructure is also very small. When the shifted composition lies at the point a" (by increasing the amount of the ternary element), the W_2C phase is completely eliminated from the microstructure and only WC-WX phases form. Examples of such microstructural evolution are seen in WC-Si and WC-B both of which easily form stable compounds with W.

4.2 Microstructure

Microstructures of the sintered samples are influenced by the heating rate, sintering temperature and time, pressure and green density. These parameters in turn affect the sample behavior at different stages of sintering. Before discussing the microstructure further, it is necessary to clarify the term, “abnormal grain growth” (AGG) associated with sintered WC. **Figure 11** shows the c/s SEM image of the edge of the WC sample where it was in contact with the graphite spacer. These regions with grain size in excess of 20 μm are instances of a particular type of AGG caused by the influence of C from the spacer during sintering[7]. Such AGG occurs only on the surface of the samples and can prove deleterious to the surface mechanical properties of the samples. Indentations on these grains resulted in a high density of small cracks and very low hardness (<1300 VH). Composition imaging of the same area showed that W was in excess in these regions indicating that the brittle W_2C phase had formed in these regions along with the large grains. This is expected to be an effect of the preparation method since with SPS the temperature at the outer boundaries of the sample is greater than the interior. This proves favourable for the formation of W_2C by a complex process of either oxidation of WC or by the decomposition of the WC_{1-x} phase as discussed in the earlier section. All the samples that contained the W_2C phase (WC- Re, Ta and Nb) showed such AGG at the surface regions. Samples that did not contain the W_2C phase (WC-Si, B) did not show any indication of AGG at the surface. In the same Fig. 11, the interior part also shows another type of abnormally long, facetted grains embedded in a uniform matrix of smaller grains. These facetted grains are also a result of AGG and occur throughout the interior of the samples due to the influence of surface and interface energies on the coarsening behavior. The abnormal growth commonly referred to in sintered WC is the second type of AGG and their formation depends primarily on the temperature and holding time[22]. Henceforth, our reference to abnormal grains will be to these large facetted grains that are seen in the interior of the samples.

In all the samples studied, three types of sintered microstructure can be discerned based on the final grain size and distribution: (i) uniform restricted grain growth (< 200 nm), (ii) uniform rapid grain growth (> 500 nm) and (iii) abnormal grain growth (including extensive faceting and anisotropic growth). All the 21 samples studied in this work fall under one of these categories.

The most desirable growth features are those described by the first type of microstructure. WC-Re, WC-Ta and WC-Nb fit into this category. As seen in the SEM micrographs, they restrict grain growth and the

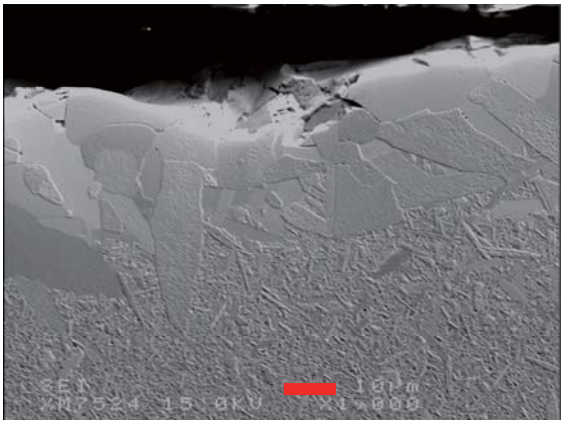

Fig. 11 AGG at the graphite/sample interface (Red marker represents 10 μm).

scatter in their grain size distribution is also narrow. Their hardness values equal that of binderless WC and their hardening behavior correlates, within experimental error, to their grain sizes according to the Hall-Petch effect. However, these samples have a primary drawback that their microstructures contain the brittle semi carbide phase resulting in low fracture toughness. Based on their final microstructure and density, it can be speculated that these samples follow a three stage sintering path[18] with no abnormalities in their sintering behavior except for the initial stage oxidation which is common to all the other samples also. From an observation of the phase diagram it is interpreted that these samples undergo complete solid state sintering. An analysis of the slope of the sintering curves of these samples (shrinkage rate) show that they exhibit a similar 3 stage sintering behavior (**Fig. 12**). The sintering rate which is initially low rises to a maximum and has a consistent high value after which it decreases rapidly. From the interrupted sintering behavior of pure nano WC[18] the first shoulder at about 800 C (indicated by vertical arrow in Fig. 12) can be attributed to particle rearrangement. This is followed by necking between the

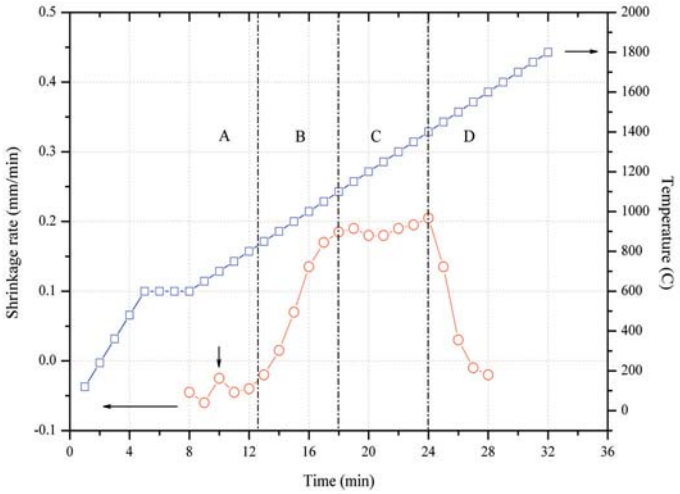

Fig.12 Sintering rate curve of samples that show restricted grain growth.

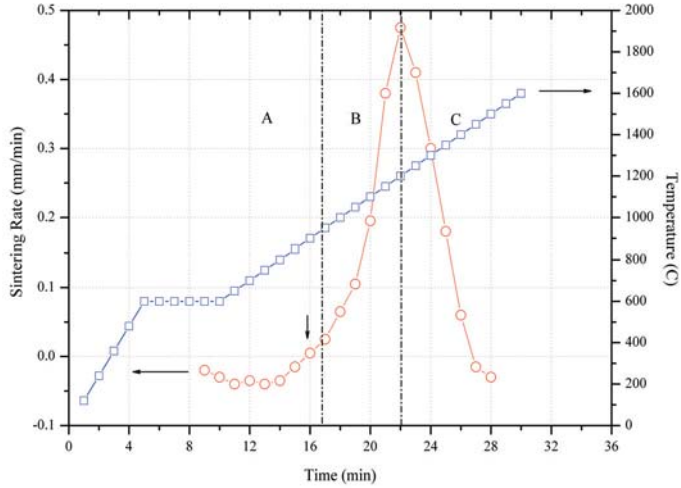

Fig. 13 Sintering rate curve of samples that show faceting and rapid grain growth by LPS.

particles which also yield negligible change in sintering rate up to 900 C. From 900 C to 1200 C there is a rapid increase in densification rate (due to change of pore shape, shrinkage and local grain growth) followed by a plateau region which can be attributed to uniform initial grain growth and annihilation of micro pores and complete compaction (the intermediate stage of sintering). This is followed by a drop in sintering rate due to significant grain growth (and isolated pore structure) at which the heating is halted.

We believe that the final plateau region is essentially what contributes to the 100% densification observed in these samples. It is in this steady densification region that the nature of the particles and the role of the ternary element as a grain growth inhibitor assume significance.

It is well known that in the conventional WC with lesser than 6 wt% Co, the low fraction of Co is accommodated in small pockets at the WC grain boundaries. During sintering, the Co spreads as a thin layer lining the WC grains[23]. Even on the addition of grain inhibitors like VC, they (VC particles) have been found to form thin layers around the WC grains, or precipitates along certain preferred planes or in small pockets at GB intersections[24]. It is assumed that in a similar way, the binders Nb, Ta and Re also spread along the surface of WC particles. At the plateau region in the sintering rate curve, the WC particles are compacted rapidly, but undergo minimal grain growth because the intervening binder acts to lower the surface energy of the WC grains. They passivate the grain boundaries by forming thin layers of carbide phases substituting for the W atoms at the WC/WC interface. This reduces the driving force for grain coalescence by retarding the nucleation rate during the final stage of sintering thus inhibiting grain growth. Such mechanisms have been reported for NbC – WC – Co compacts[25].

The sintering rate curves of WC-Si, WC-Ti and WC-B differ from that of the other ternary additions by the absence of the plateau region (**Fig. 13**). Nevertheless, the initial part of the curve is similar up to the point of rapid densification. After 1200 C, the densification rate decreases gradually at first and then drops rapidly up to the temperature at which sintering is completed. This means that from 1200 C to the completion of sintering, the heat energy is used not only for densification, but also for other mechanisms namely phase transformation and grain growth. It is believed that these samples underwent liquid phase sintering. The melting point of Si (1420 C) and Ti (1670 C) are very near their respective sintering temperatures (1400 C and 1650 C respectively). In the case of WC-B it is suspected that the oxidized compound B_2O_3, owing to its high vapour pressure, melts and evaporates during this temperature range providing the liquid phase for sintering. Moreover, with SPS, the local temperature could be very high due to intense arcing between particles. This enhances the solution – re-precipitation process of grain coarsening (Ostwald ripening mechanism) which leads to a rapid grain growth at the final stages of sintering. WC-Ti2 and WC-B

showed similar type of microstructure with large porosity. In the case of WC-Ti2, the high sintering temperature of 1800 C was sufficient to evaporate the TiO_2 leaving a porous microstructure. In both these systems, the recorded density and hardness was very low. However, WC compacts which have a tendency to show abnormal and facetted grain growth, showed a uniform grain size distribution with the addition of Boron. We suspect that this is due to the production of boron oxide which neutralizes the anisotropy in the GB energies of WC crystals.

The WC-Si system also showed an interesting microstructure. The fractured surface showed two types of grain morphologies: small facetted grains with longitudinal structure (aspect ratios between 2 and 3) and very large plate shaped grains (aspect ratios exceeding 4). Some of the large grains are also seen to be composed of neatly stacked sub-grains. However, the conventional coarsening theory cannot account for the strong anisotropic growth behavior observed in WC-Si samples. It is now generally accepted that the AGG in WC composites is a result of anisotropy in GB energies. Even if the difference in surface energies and packing density between the prismatic (10-10) and the basal (0001) planes are considered, a truncated triangular shaped morphology is to be expected by sintering. The observed microstructure indicates that the thickness along the [0001] direction is around 500 nm while the prismatic planes exceed 2 μm. Such high aspect ratios are not seen in the pure WC samples. This unique growth behavior can be explained only if there is a local alteration of the surface energies by interfacial reactions between WC and Si. It is believed that during the early stage of sintering, Si attaches to the WC cell to form the congruently melting W_5Si_3 (ΔG = -150 kJ/mol) compound. It is then possible that initially a region where Si had deposited can act as a 2D nucleation site for grain growth and contiguous grains can easily coarsen to form abnormal structures. At the later stages of sintering, facetted WC grains with their prismatic or basal planes adjacent to each other also coalesce rapidly leading to the excessive growth of plate shaped or layered grains with intermittent porosity. Generally, it appears that during sintering, grain coarsening, coalescence and defect assisted abnormal growth occurs in the WC-Si sample.

Recently, Zhang et al[26] have reported hexagonal platelets in WC-Co-1% Y_2O_3 cemented carbides. However they attribute it to the coherency between the WC/Co interfaces. As the fraction of binder phase increases the number of WC/binder interfaces exceeds that of WC/WC interfaces. In this case, we believe that the kinetics of longitudinal growth can be better described by a preferential WC/Si interface controlled growth which alters the GB energy of WC crystals. Although the Si content was low, melting of Si allows the binder to spread, thus influencing the microstructure throughout the sample. The extensive amount of pores seen along the longitudinal direction and their shapes (some pores are rectangular) also clearly indicate that sintering had occurred by the stacking – type coalescence of large grains rather than curvature – driven coarsening of small grains.

Nevertheless, irrespective of the additive used, it is established that the presence of the liquid phase significantly alters the morphology of the grains during SP sintering of WC.

5. Conclusions

In the present study, we found that *n*-WC powders can be spark plasma sintered with constrained grain sizes in the range of 160 – 250 nm. Higher heating rates yield consistently high density and small grain size. For the pure WC, WC-Re and WC-Nb, full densification could be achieved together with limited grain growth. This proves their potential as grain growth inhibitors in the sintering of WC. For WC-Si, Ti and B which form reactive phases with WC, temperatures lower than 1400 C is recommended to avoid excessive grain growth. These results suggest improved grain size control by combined high pressure-low temperature sintering of WC.

References

1) Bartha L, Atato P, Toth A L, Porat R, Berger S, Rosen A, *J. of Adv. Mat.*, **32-3**, 2000, pp. 23-26.
2) Agrawal D, Cheng J, Seegopaul P, Gao L, *Pwd. Metall.*, **43-1**, 2000, pp. 15-16.
3) Breval E, Cheng J P, Agrawal D K , Gigl P, Dennis M, Roy R, *Mat. Sci. and Eng. A*, **391,1-2**, 2005, pp. 285 -295.
4) Kim H C, Oh D Y, Shon I J, *Int. J. of Refractory Metals and Hard Materials*, **22, 4-5**, 2004, pp. 197 - 203.
5) Schubert W D, Neumeister H, Kinger G and Lux B, *Int. J. of Refractory Metals and Hard Materials*,**16**, 1998, pp. 133-142.
6) M. Sherif El-Eskandarany, Amir A. Mahday, H. A. Ahmed, A. H. Amer, *J. of Alloys and Compounds*, **312, 1-2**, 2000, pp. 315-325.
7) Luca Girardini, Mario Zadra, Francesco Casari and Alberto Molinari, *Metal Powder Report*, **63-4**, 2008, pp. 18-22.
8) Hwan CHeol Kim, In-Jin Shon, Jin – Kook Yoon and Jung-Mann Doh, *Int. J. of Refractory Metals and Hard Materials*, **25**, 2007, pp. 46-52.
9) Jiuxing Zhang, Guozhen Zhang, Shixian Zhao, Xiaoyan Song, *J. of Alloys and Compounds*, **479**, 2009, pp. 427-431.
10) V. B. Voitovich, V. V. Sverdel, R. F. Voitovich, E. I. Golovko, *Int. J. of Refractory Metals and Hard Materials*, **14-4**,1996, pp. 289-295.
11) Huilong Zhu and Averback R S, *Phil. Mag. Letters*, **73-1**, 1996, pp. 27-33.
12) Seong Jin Park, Kristina Cowan, John L. Johnson and Randall M. German, *Int. J. of Refractory Metals and Hard Materials*, **26-3**,2008, pp. 152-163.
13) Hwan-Tae Kim, Dong-Wook Choi, Ji-Soon Kim, Young-Soon Kwon, Hye-Suk Kwon and Eung – Ryul Baek, *Proc. of 7th Korea-Russia Int. Symp. on Sci. and Tech.*, **1**, 2003, pp. 56- 62.
14) Huang B, Chen L D, Hai S Q, *Scripta Materialia*, **54**, 2006, pp. 441-445
15) Tao Li, Qingfa Li, Fuh J Y H, Poh Ching Yu, Lu L and Wu C C, *Mat. Sci. and Eng. A*, **445-446**, 2007, pp. 587 - 592.

16) Jayaram V, *Acta Metall*., **35-6**,1987, pp. 1307-1315.
17) Swinkles F B and Ashby M F, *Acta Metall*., **29**, 1981,pp. 259-281.
18) Goren-Muginstein G R, Berger S and Rosen A, *Nanostrctured Materials*, **10-5**,1998, pp. 795-804.
19) Nanda Kumar A K, Unpublished work.
20) Azadmehr A and aheri-Nassaj E, *J. of Non-Crystallie Solids*, **354-27**,2008, pp. 3225-3234.
21) Allibert C H, *Int. J. of Refractory Metals and HardMaterials*, **19-1**, 2001, pp. 53-61.
22) Seung I. Cha and Soon H. Hong , *Mat. Sci. and Eng.* , **356, 1-2**, 2003, pp. 381-389.
23) da Silva A G P, Schubert W D and Lux B, *Materials Rsearch*, **4-2**,2001, pp. 59-62.
24) Lay S, Hamar-Thibault S and Lackner A, *Int. J. of Refractory Metals and Hard Materials*, **20-1**, 2002, pp. 61-69.
25) Huang S G, Liu R L, L L, Van der Biest O and Vleugels J, *Int. J. of Refractory Metals and Hard Materials*, **26-5**, 2008, pp. 389-395.
26) Zhang Li, Chen Shu, Wang Yuan-jie, Yu Xian-wang and Xiong Xiang-jun, *Trans. Nonferrous Metals Soc. China*, **18**, 2008, pp. 104-108.